Potential of Mean Force for Face–Face Interactions between Pairs of 2:1 Clay Mineral Platelets

Hejian Zhu, Andrew J Whittle, Roland JM Pellenq

LANGMUIR

pubs.acs.org/Langmuir Article

Potential of Mean Force for Face−Face Interactions between Pairs of 2:1 Clay Mineral Platelets

Hejian Zhu,* Andrew J. Whittle, and Roland J.-M. Pellenq

Cite This: *Langmuir* 2022, 38, 13065−13074 Read Online

ACCESS | Metrics & More | Article Recommendations | Supporting Information

ABSTRACT: Bottom-up modeling of clay behavior from the molecular scale requires a detailed understanding of the free energy between pairs of clay platelets. We investigate the potential of mean force (PMF) for hydrated clays in face-to-face interactions with free energy perturbation (FEP) methods through molecular dynamics simulations using simple overlap sampling (SOS). We show that PMF results for open systems with one finite in-plane dimension are affected by migration of counterions from within the interlayer space compared with fully confined closed system conditions. We compare PMFs for two common 2:1 clay sheet minerals Illite (IMt-1) and Na-smectite. The PMFs for the open illite systems exhibit a strong attractive energy well at a basal layer separation, d = 11 Å and interlayer water content, w_{IL} = ∼0.4% while the attractive minimum for the closed system occurs at d = 12 Å, w_{IL} = 3.5%. In contrast, net repulsion occurs between pairs of Na-smectite platelets for both open and closed systems (for d < 15−16 Å). The free energy is closely related to the distribution of counterions; while K^+ ions are bound closely to the surfaces of the illite platelets, Na^+ ions are more spatially disperse. This PMF results contradict prior findings for Na-smectite and prompted further comparisons with other published results. We find that most of the published results do not represent accurately the free energy for face−face interactions between pairs of clay platelets that are effectively infinite (with width/thickness O[10^4]). The PMF results presented in this paper form a reliable basis for mesoscale, coarse-grained modeling of illite and smectite particle assemblies. We show that the Gay−Berne potential provides a reasonable first-order model for upscaling, while the solvation potential proposed by Masoumi enables a more accurate representation of the computed PMFs.

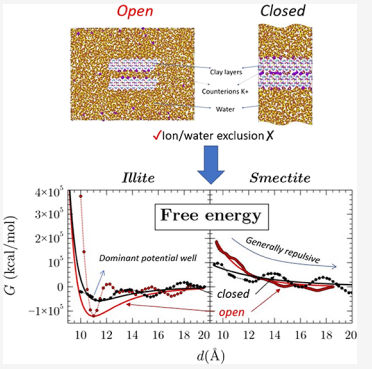

1. INTRODUCTION

Hydrous phyllosilicates are the most abundant secondary minerals found in soils and constitute up to 35% by weight of sedimentary rocks.[1] The principal groups comprise colloidal-size crystalline silicate sheets (with plan dimensions <2.0 μm), typically arranged in 1:1 or 2:1 configurations with aluminum hydroxide sheets. Clay minerals are characterized by large specific area and isomorphous substitutions in their crystalline structure that give rise to unbalanced surface charges (and determine their cation exchange capacity) and associated double layers on the mineral surfaces when exposed to aqueous electrolyte solutions.[2] Clay primary particles are found with residual soils and sediments in a variety of particle assemblages (variously referred to as flocs, clusters, and/or aggregates in the literature) with characteristic length scales ranging from 10 to 100 μm. For clarity, in the following discussions, a single 1:1 or 2:1 layer is referred to as a primary particle or platelet, and the ordered assemblies of primary particles are called aggregates. The smallest of these units are typically associated with face−face particle arrangements. Intercalation of water molecules between individual sheets of smectite (osmotic hydration)[3] is well known as the source of volume change/swelling in smectites while other 2:1 minerals such as illite typically have higher surface charge density[2] and are able to form larger, stable aggregate stacks or crystallite laths.[4,5]

Bottom-up, multiscale computational modeling aims to describe the particle arrangements and pore structure of clays in order to understand the physics underlying macroscopic mechanical, flow, and transport properties. Much progress has been made in atomistic modeling of clay−aqueous solution interactions through using generalized interatomic potential functions, such as ClayFF[6] that represents atomic interactions within the clay using (i) nonbonded potentials (Lennard-Jones and Coulomb), (ii) harmonic bond and bond-angle potentials for hydroxyl (and optionally metal-oxygen-hydrogen) groups, and (iii) an extended simple point charge model for water molecules (SPC/E).[7] For example, Underwood and Bourg[8] described large-scale molecular dynamics (MD) simulations (over a time period of ∼150 ns) of the particle arrangements due to dehydration of smectite for an initially random distribution of 30 hexagonal clay particles (each with side length ∼60 Å)

Received: June 21, 2022
Revised: September 26, 2022
Published: October 20, 2022

solvated in water in a system containing more than 2.4 M atoms. It is clear that there are practical limits to the size of these models and a coarse-graining approach is needed to characterize the behavior for larger-scale particle assemblages and over much longer time frames. In prior work, we[9] proposed a scheme based on a free energy perturbation method for establishing the potential of mean force (PMF) between pairs of clay primary particles interacting in face−face and edge−edge configurations. By calibrating the PMF results to analytical potential functions, it is then possible to upscale directly to much larger mesoscale particle assemblages.[10]

This paper revisits the calculation of PMFs for clay primary particles, provides new insight into effects of ion exclusion within the interlayer space, and compares the behavior for two reference 2:1 clay minerals, sodium smectite and illite. We compare results with published PMFs for face−face interactions and identify suitable analytical interparticle force models to represent this behavior in mesoscale simulations.

2. METHODOLOGY

2.1. Molecular Model of 2:1 Clays. We use the chemical structure of Montana illite (IMt-1)[11] and Wyoming montmorillonite (Na-MMT Wyo)[12] as the two reference materials. IMt-1 has isomorphous substitutions in all three constituent layers (Si → Al in tetrahedral layers; Al → Mg and Fe(III) in the octahedral layers) such that the individual primary particle has a surface charge density of 0.296 C/m^2. Na-MMT Wyo also has isomorphous substitutions in both tetrahedral (Si → Al) and octahedral (Al → Mg) layers but a much lower surface charge density 0.127 C/m^2 (and a widely reported CEC = 104 meq/100 g).[13] The current analyses use K^+ ions to achieve charge neutrality for IMt and Na^+ for Na-MMT.

The molecular models for the reference clay minerals in molecular simulations are developed by introducing isomorphous substitutions to the atomistic structure of a charge-neutral mineral pyrophyllite.[14] The resulting chemical compositions are close to the real source clay:

$$\mathrm{IMt-1:\ K_{1.75}[Al_{2.75}Fe(III)_{0.75}Mg_{0.5}][Si_{6.75}Al_{1.25}]O_{20}(OH)_4} \quad (1a)$$

$$\mathrm{Na-MMT:\ Na_{0.75}[Al_{3.5}\ Mg_{0.5}][Si_{7.75}Al_{0.25}]O_{20}(OH)_4} \quad (1b)$$

The atoms interact through ClayFF force field,[6] which has non-bonded interactions in the form of short-range Lennard-Jones potentials and long-range Coulomb potentials and harmonic bonded interactions in hydroxyl groups, with water molecules represented using the extended simple point charge model (SPC/E).[7] This representation has been widely used in the study of clay minerals and has been verified against experimental measurements of their crystalline structures[15−19] and elastic properties.[20,21] More details can be found in Appendix A. The isomorphous substitutes are randomly distributed within the tetrahedral and octahedral sheets subject to the constraints imposed by Lowenstein rules.[5]

There has been extensive research to understand the reactivity of the edge surfaces of 2:1 clays, which affects colloidal stability and rheological properties.[22] The current analyses truncate the [010] edge sites and saturate the broken bonds with H or OH based on the structure provided by ab initio simulations by refs 23, 24, as shown in Figure 1a. Edge corrections introduce $H_{32}O_{16}$ extra atoms on each platelet of 640 atoms (with a typical size of 20.87 Å (x) × 36.32 Å (y) × 6.73 Å (z)). The added oxygen atoms have the same partial charges as the usual hydroxyl oxygens. It is important to maintain the same total number of atoms among all systems for a valid comparison of the results. To keep the number of counterions the same, i.e., the total charge of the platelets unchanged by the edge corrections, we redistribute a partial

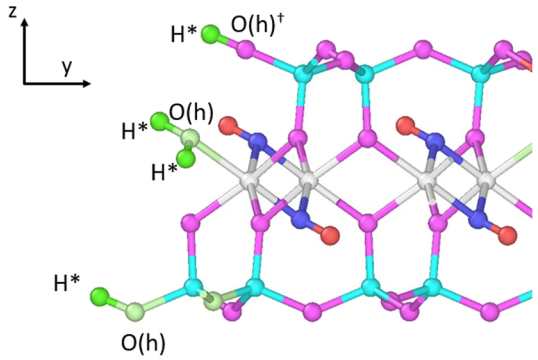

(a) Edge correction

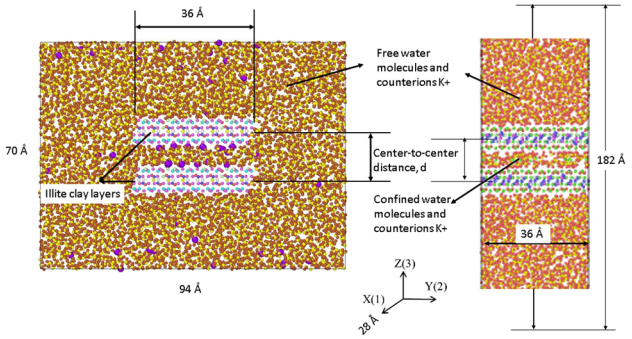

(b) Face-face interactions for open (o-F-F) and closed (c-F-F) systems

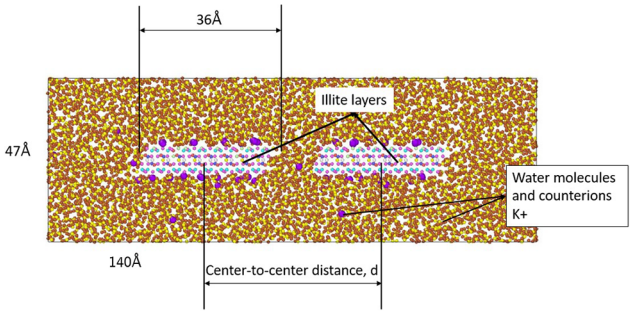

(c) Edge-edge interactions

Figure 1. Representations of the atomistic systems. (a) Added and replaced atoms at the edges of the clay particles for face−face open systems and for edge−edge systems. O(h) means oxygen atoms in hydroxyl groups. *Partial charges for edge hydrogen atoms are adjusted to 0.45e for smectite and 0.44e for illite. †The oxygen atoms are originally O(b) (bridging oxygen atoms) or O(s) (bridging oxygen atoms neighboring a substitution). They are changed to O(h) to represent the chemistry of edge sites. The other two figures show the front view of the simulation cells for PMF analyses for illite−water systems: (b) open and closed systems for face−face interactions and (c) edge−edge configurations. Free energy is obtained at selected separations, d_i. Periodic boundary conditions are applied for all cases.

https://doi.org/10.1021/acs.langmuir.2c01632
Langmuir 2022, 38, 13065−13074

charge to the edge H atoms of 0.45e for Na-MMT and 0.44e for IMt.

2.2. PMF from the FEP Approach. Atomistic models for two platelets were located at a specified separation within the unit cell simulation box using periodic boundary conditions in all three directions. Each system was then solvated with the same number of water molecules (3914) and subjected to isothermal isobaric relaxation at 300 K and 1 bar for 500 ps. This was followed by a 3000 ps production period at constant temperature (300 K) constant volume and fixed clay layer separation (d_i). At each separation distance, we generated 3000 copies of equilibrated configurations for free energy calculation. The analyses were carried out using open-source LAMMPS software[25,26] and used OVITO software[27] for visualization. The interatomic interactions are defined by the ClayFF force field.[6] In the LAMMPS implementation, the short-range van der Waals interaction in the LJ form were cutoff and shifted at 8.5 Å. The long-range Coulombic interaction was calculated with the particle-particle-particle-mesh (PPPM) Ewald summation method.[28] The temperature and pressure control in molecular dynamics (MD) simulations are performed through a Nosé−Hoover thermostat and the Parinello−Rahman barostat.[29]

Following Ebrahimi and co-workers,[9] we use a free energy perturbation method for face−face (F−F) and edge−edge (E−E) configurations (Figure 1b,c). F−F interactions can be analyzed using either open or closed configurations (Figure 1b). The closed configuration (c-F−F) represents infinite platelets where there is no migration of counterions or water molecules between the confined interlayer space (between the two primary particles) and the exterior space. The open system (o-F−F) represents particles that have one infinite (x) and one finite (y) in-plane dimension. Counterions and water molecules can migrate to and from the interplatelet space. Due to the introduction of extra H and O atoms at the edges, the number of water molecules reduced by 32 in o-F−F and E−E systems (3914 water molecules in c-F−F systems and 3882 in o-F−F and E−E systems). The simulation boxes are sized to shield interactions between the platelets and their periodic image and to ensure that water molecules close to the exterior boundary approximate the behavior of bulk water under standard temperature and pressure (with bulk density 0.996 g/cm^3).

The free energy perturbations (FEP) calculations consider a set of initial separation distances, d_i, referred to as a 'state' in the following discussions. We perturb the equilibrated configurations of each state obtained from the MD trajectory, forward and backward, by a specified increment of the separation distance, $\delta_{\pm} = d_{i\pm1} - d_i$. The changes in potential energy ΔU effected by the perturbation are recorded and used to calculate the free energy difference between adjacent states, through the simple overlap sampling (SOS) formulation:[30−32]

$$\Delta G(d_i \rightarrow d_{i\pm1}) = -\frac{1}{\beta}\ln\left[\frac{\langle \exp(-\beta\Delta U(i \rightarrow i \pm 1)/2)\rangle_i}{\langle \exp(-\beta\Delta U(i \pm 1 \rightarrow i)/2)\rangle_{i\pm1}}\right] \quad (2)$$

where $b = 1/(k_B T)$, k_B is Boltzmann's constant and T is the temperature in K. $\langle \cdot \rangle_i$ refers to the ensemble average over the equilibrated configurations for state i. Throughout the perturbation calculations, the bond lengths and bond angles of water molecules are fixed with SHAKE algorithms[33] in LAMMPS. The series of free energy differences can be connected to a full free energy landscape with respect to the separation distance between primary particles with an assumed zero level at the largest separation. More details are provided in Appendix C.

3. RESULTS AND DISCUSSION

3.1. Illite. Figure 2 summarizes the Gibbs free energy per unit area (G/A) in F−F interactions between illite platelets

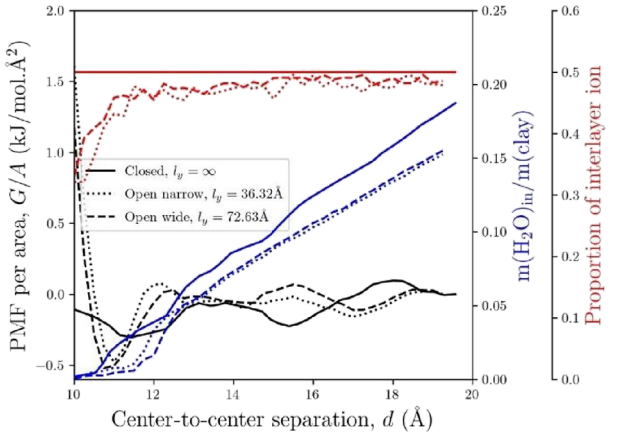

Figure 2. PMFs for face−face interactions between illite particles computed using the free energy perturbation approach, comparing open configurations (finite l_y with free migration of counterions) with a closed configuration ($l_y = \infty$).

from two open configurations with l_y = 36.3 and 72.6 Å and the closed system ($l_y = \infty$) for basal layer separations ranging from d = 10−20 Å. The results show a net attractive energy well at d = 11.0−11.5 Å for all three configurations and periodic oscillations in free energy extending to d = 19 Å (with characteristic wavelength ∼3 Å). The potential well is most pronounced for the open systems, suggesting that the width of the illite particle (l_y) affects the free energy. As $d \rightarrow$ 10 Å, all three systems approach a condition where the interior water content $m_w/m_c \rightarrow 0$ while only 30% of the counterions remain in the interlayer space of the open systems. As a result, the open systems exhibit net repulsion (as $d \rightarrow$ 10 Å) while the closed system has net face−face attraction.

Differences in the results for the three configurations can be linked to the mass of water $(m_w/m_c)|_{IN}$ and fraction of the K^+ counterions in the interlayer space. The closed system allocates 50% of the counterions in the interlayer space for all basal separations while ion exclusion occurs in the open systems and is most noticeable at basal separations, $d \leq$ 11 Å. The closed system has a higher water content in the interlayer space for all separation distances, and the open systems have very low water content $(m_w/m_c)|_{IN} < 0.01$ at $d <$ 12 Å.

3.2. Smectite. Figure 3 summarizes the computed PMF for F−F interactions between a pair of Na-smectite platelets (with Na^+ counterions) based on similar free energy perturbation analyses. The results show net repulsive free energy between the particles with separations $d <$ 16 Å, and only a small net attraction energy well in the open system (l_y = 36.32 Å) at d = 17.25 Å. The closed system shows small oscillations in the free energy field with local minima at d = 12, 16 Å. In this case, ion exclusion effects occur in the open system at all separation distances (at d = 20 Å, only 42% of the Na^+ ions are in the interlayer space), while the two systems have a rather similar water content at small spacing ($d <$ 11 Å). The results in

https://doi.org/10.1021/acs.langmuir.2c01632
Langmuir 2022, 38, 13065−13074

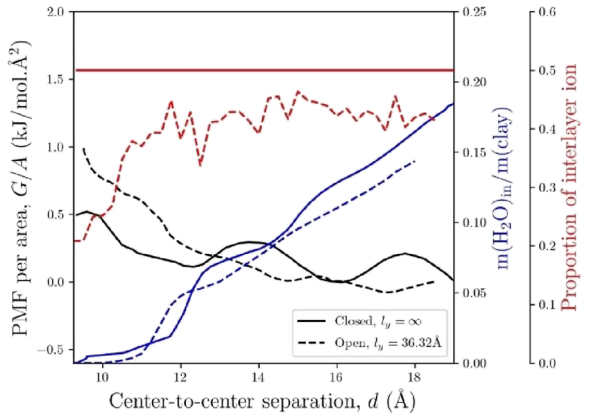

Figure 3. Comparison of PMFs for face−face interactions between Na-smectite platelets in open and closed configurations (Wyoming montmorillonite with Na^+ counterions).

Figure 3 differ significantly from prior PMF results reported by Ebrahimi and co-workers[9] that used a similar method of analysis for the closed system (here, we report recomputed PMFs from the water content data provided by Ebrahimi and co-workers;[9] Appendix B provides a direct comparison with this earlier study) and has provoked a more detailed investigation of other results reported in the literature.

3.3. Ion Distribution. In order to further understand the effect of counterions on the F−F interaction between the primary particles, Figure 4a,b compares the distributions of counterions along the axis of basal layer separation (z axis) for the illite and Na-smectite systems. At a separation distance, d = 16.9−17 Å, the K^+ ions are positioned within very narrow bands along each of the 4 surfaces of the clay platelets (Figure 4a, for both open and closed configurations). As the separation distance is reduced to d = 11−11.5 Å, the counterions located align along the midplane between the platelets. In contrast, there is a much wider distribution of Na^+ ions around the Smectite particles at both separation distances (Figure 4b).

These observations are consistent with prior studies using MC and MD methods for illite[34,35] and Na-smectite.[20,36] This implies that the surrounding molecules are more closely bound to the surface of illite than Na-smectite, partly due to the higher surface charge density and partly due to the differences in the physicochemical properties of K^+ and Na^+ ions. As two primary particles are brought together, illite tends to have stronger repulsion in the near field while the far field interaction is weaker than smectite. This is consistent with the observation in the decomposition of the PMFs presented below (Section 4.2).

The wider distribution of Na^+ ions near the surface of smectite particles also gives rise to more prominent ion exclusion effects at larger separation distance.

3.4. Comparison with Prior Studies. Our review has identified 7 prior studies that consider free energy between Na-smectite platelets (Table 1). These differ in the methods of analyses, geometry, force fields, and clay mineralogy used. Three different methods of analyses have been used: The first[37−40] uses grand canonical Monte Carlo (GCMC) simulations to solvate the system through equilibrating the interlayer space with an implicit water reservoir of specified chemical potential or pressure. MD simulations are then conducted to compute the disjoining pressure in the interlayer space between the platelets using NVT simulations. The

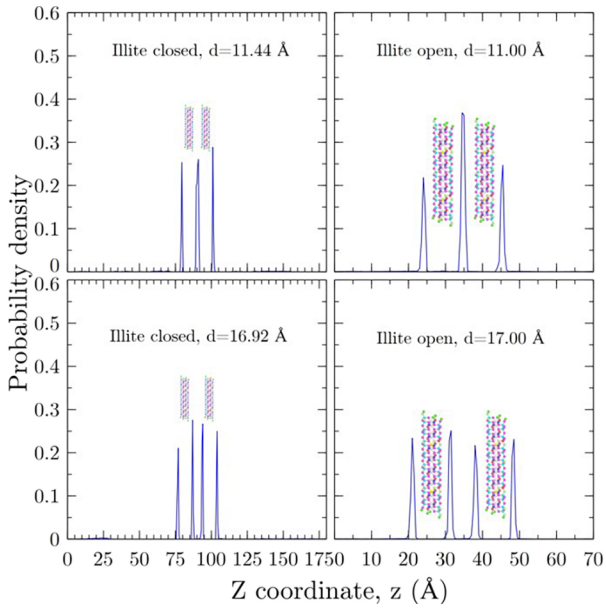

(a) Illite K^+ counterion distribution

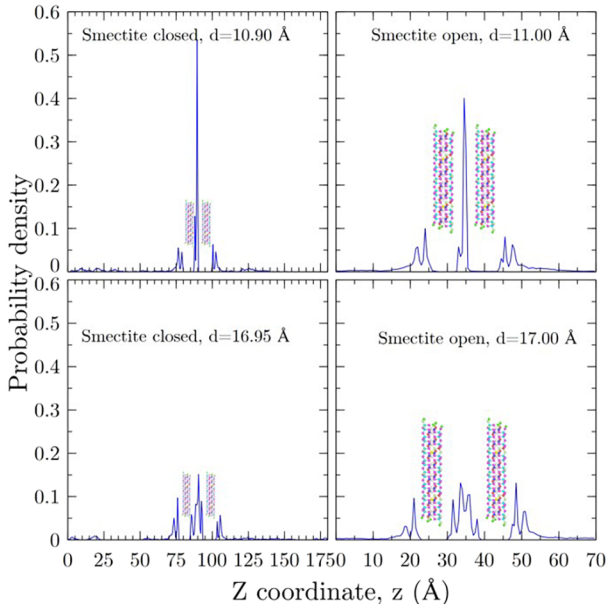

(b) Na-Smectite Na^+ counterion distribution

Figure 4. Ion distribution in the direction perpendicular to the clay primary particles. All results are averaged over 1000 configurations from the MD trajectory of 1 ns in the equilibrated stage. For closed systems, the region under consideration is the entire simulation box; for open systems, the results consider only $|l| \leq |l_y|$.

combination of the MC and MD simulations is customarily referred to as $\mu_w VT$ or osmotic ensemble.[41] The pressure, p_z, (strictly speaking the normal stress component in the z direction) is computed through a standard virial expansion and can be related to the free energy per unit area, G/A as follows:

$$G/A = \int_{\infty}^{d} p_z \, dz \tag{4}$$

All these analyses consider using periodic boundaries in all directions, effectively simulating platelets of infinite dimensions

https://doi.org/10.1021/acs.langmuir.2c01632
Langmuir 2022, 38, 13065−13074

Table 1. Specifications of the Methods Reported for PMF Computations in the Literature[e]

source[d]	method	type	force field	#	L_x (Å)	L_y (Å)	d (Å)	Box [x, y, z] (Å)	T (K)	P (MPa)
Whitley (WS04)	MC&MD	Az	Skipper[a]	∞	∞	∞	12.0−18.5	21.2, 18.3, d	298	0.1
Honorio (HBV17)	MC&MD	Wy	ClayFF	∞	∞	∞	9.7−19.0	20.7, 18.0, 2d	300	2−200
Brochard (B21)	MC&MD	Wy	ClayFF	∞	∞	∞	9.25−23.25	20.6, 17.9, d	300	2−200
Svoboda (SML18)	MC&MD	Wy	ClayFF	∞	∞	∞	10.0−31.0	20.74, 35.94, 2d	365	27.5
Ho (HCG19)	Colvars[b]	Az	ClayFF	2	∞	31	9.5−16.5	100.0, 31.1, 73.6	300	0.1
Shen (SB21)	Colvars[c]	Az'	ClayFF	2	60(hex)	60	12.0−40.0	100.0, 100.0, 103.0	300	0.0
Ebrahimi (EWP14)	FEP	Wy	ClayFF	2	∞	∞	9.25−18.5	20.9, 36.3, 179.6	300	0.1
Current (ZWP22-c)	FEP	Wy	ClayFF	2	∞	∞	9.25−18.5	20.9, 36.3, 179.6	300	0.1
Current (ZWP22-o)	FEP	Wy	ClayFF	2	∞	36.3	9.25−18.5	20.9, 94.0, 70.0	300	0.1

[a]Force field by Skipper and co-workers.[61] [b]With umbrella sampling. [c]With metadynamics, Shen considers hexagonal clay crystals and uses a slightly higher surface charge for Arizona montmorillonite than Ho. [d]The papers are listed by the name of the first author for brevity. [e]Abbreviations are the following: MD = molecular dynamics, MC = Monte Carlo, Colvars = collective variables, FEP = free energy perturbation. Unit cell formulae for clays: Az: $Na_{0.75}[Si_8][Al_{3.2}Mg_{0.8}]O_{20}(OH)_4$; Az': $Na_{0.8}[Si_8][Al_{3.25}Mg_{0.75}]O_{20}(OH)_4$; Wy: $Na_{0.75}[Al_{3.5}Mg_{0.5}][Si_{7.75}Al_{0.25}]O_{20}(OH)_4$.

while ratios of the separation distance to box size (z dimension; Table 1) correspond to simulations for an infinite assembly of platelets rather than the pair of platelets considered above.

A second group of studies[42,43] uses the collective-variable based methods to compute the potential energy landscape with respect to a reaction coordinate by probing using a biased sampling method (umbrella sampling and metadynamics, respectively). These sampling methods ensure that the parts of the landscape corresponding to less likely cases can also be probed by the MC or MD trajectories, through application of a bridging weighting function[42] or through adding bias potentials to the real free energy.[43] This type of method has the ability to probe a large range of landscapes, but the accuracy is highly dependent upon the *a priori* choice of sampling parameters (e.g., the weighting function and the rate of application of the bias potentials) and can be computationally expensive. The analyses by Ho and co-workers[42] considered interactions between pairs of smectite platelets with one infinite in-plane dimension (geometrically similar to the open system analyzed by FEP, Figure 1b) while Shen and Bourg[43] simulated interactions between a pair of hexagonal platelets (with uncharged cleaved edges after White and Zelazny[44]).

All of the prior analyses, except Whitley and Smith,[37] use the ClayFF force fields for the smectite and SPC/E for water molecules with Na^+ counterions. However, there are differences in the isomorphous substitutions and surface charge density: Whitley and Smith,[37] Ho and co-workers,[42] and Shen and Bourg[43] simulated smectite with isomorphous substitutions only in the octahedral layers (Al → Mg), which is sometimes referred to as Arizona montmorillonite, while Honorio and coworkers,[38] Ebrahimi and co-workers[9] and the current study include IS in both tetrahedral and octahedral layers (Wyoming montmorillonite). The surface charge densities for Az and Wy montmorillonite are similar (overall valence −0.75e per unit cell) for most cases while Shen and Bourg[43] used a structure (Az′) with slightly higher charge density (−0.8e per unit cell).

Figure 6 compares the PMF free energy curves for face−face interactions between from these published papers. In general, open systems (e.g., HGC19 and ZWP22-o) have larger repulsion at smaller separation and no dominant potential wells while closed systems (WS04, HBV17, B21, EWP14, and ZWP22-c) exhibit more prominent oscillatory features. The position of the potential wells for the closed systems are not exactly aligned but all are approximately at 12, 15.5, 19 Å, etc., corresponding to the formation of one, two, and three structured water layers in the interlayer space. Prior experimental works using X-ray diffraction (XRD) methods showed similar results. For example, Ferrage and co-workers[16,17] showed that, in the case of Na-smectite, one, two, and three water layers correspond to layer separations of 11.6−12.9, 14.9−15.7, and 18−19 Å. Among the results from osmotic ensemble simulations (i.e., MC + MD), different clay types and force fields did not affect the general trend. Higher reservoir pressure (HBV17, SML18, Table 1) for the interlayer water also had little influence on the reported PMF.

The results of HCG19 and SB21 are not consistent as claimed[43] but exhibit diverging trends at smaller separations, which could be the result of differences in particle size and/or charge density. The FEP results of Ebrahimi and co-workers[9] and ZWP22-c (both closed systems, differing only in the interlayer water content) exhibit similar spatial landscapes of normalized free energy for d > 13 Å, but only the prior results[9] show net attraction at small separation distances (well-defined attractive potential well at d = 11.75 Å).

In contrast to smectite, traditional XRD experiments measure monodispersed layer separation for illite/mica minerals[45−47] for 0 water layers at around 10 Å. The FEP results for open and closed systems in this work shows a global minimum at 11 and 11.5 Å, with a small amount of water molecules in the interlayer space. The differences arise from the differences in the thermodynamics status between the real and simulated systems. In the conventional XRD measurements on illite/mica, air-dried or naturally dried samples are used, where the water content of the sample is usually at a very low level and the pore space is subjected to an unsaturated surrounding environment (with relative humidity <100%). More recent research studies on synthetic mica-type materials with more homogeneous chemical composition and saturated surrounding environment[48−50] showed larger dominant d001 separation for 0/1 W ranging from 10 to 12 Å and also less prominent peaks showing 2 W layer separation ranging from 13.2 to 14.7 Å at a higher level of bulk water content. The simulation findings for illite are consistent with these values.

From the result of the F−F PMFs, we have estimated the elastic stiffness of the platelet-pair system in the direction perpendicular to the particle plane near the equilibrium positions. The C_{33} stiffness component can be obtained by direct numerical differentiation of the free energy:

https://doi.org/10.1021/acs.langmuir.2c01632
Langmuir 2022, 38, 13065−13074

$$C_{33} = \frac{d}{A}\frac{\mathrm{d}^2 G(d)}{\mathrm{d}d^2} \tag{3}$$

We have estimated the values at the local minima of the PMF curves for the illite closed and open systems, and the smectite closed systems. As there are no prominent minima for the open-smectite systems, we estimated C_{33} values from states with maximum local curvature. The results are presented in Figure 5, together with the experimental data from previous

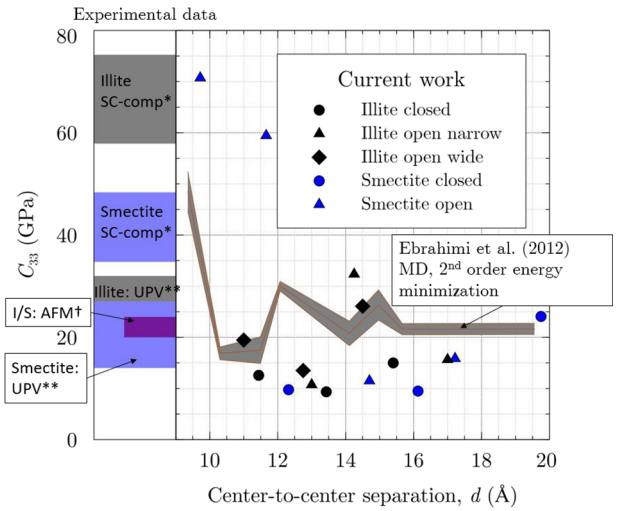

Figure 5. Elastic stiffness in the direction perpendicular to the particle planes for F−F systems. Results shown are for separations corresponding to major local potential wells (in the cases of illite closed and open and smectite closed systems) and the positions with maximum curvature in PMF curves (for smectite open systems). Comparison with experimental data from previous research studies[20,51−53] are also included: *from Wang et al.;[51] **from Ortega et al.;[52] †from Graham et al.[53] The shaded band represents data obtained through second-order minimization of atomistic systems using GULP.[62]

simulation and experimental studies, including the molecular simulation results through second-order energy minimization by Ebrahimi et al.[20] The accuracy of the second-order derivative (eq 3) is limited by the grid spacing in the PMF calculations and the accuracy of the computed free energy. In terms of the order of magnitude, the resulting values are reasonably consistent with previous simulation results for smectite.[20]

The experimental data include self-consistent estimates of effective moduli from elastic wave velocity measurements in clay−epoxy composites,[51] UPV measurements on natural clay shales,[52] and AFM measurements on the mixed-layer illite/smectite phase of shale.[53] While the AFM and UPV data are in reasonable agreement with the computed values of C_{33}, the reported values of effective modulus from self-consistent elastic bounds in clay−epoxy composites are much higher. This may be partly attributed to dehydration of the clay in these tests (as noted by Wang et al.[51]). It should also be noted that the macroscopic experiments in composites (and other UPV tests) measure properties of particle assemblies (with a range of orientations) at a much larger length scale than the current MD simulations for the platelet-pair system.

3.5. Coarse-Grained Representation of Clay Platelets.

3.5.1. Gay−Berne Potential. Mesoscale simulations are accomplished by coarse-graining the nanoscale PMF results to represent interactions between assemblies of clay particles. In prior research,[9] clay platelets were represented as single-site ellipsoidal disks (with dimensions; $[a_i, b_i, c_i]$) that interact with each other through the Gay−Berne potential function (GB):[54−56]

$$U = 4\varepsilon\left[\left(\frac{\sigma}{h_{12}+\sigma}\right)^{12} - \left(\frac{\sigma}{h_{12}+\sigma}\right)^{6}\right]\eta_{12}\chi_{12} \tag{5a}$$

where ε = 1 kcal/mol sets the energy unit, σ is the atomic interaction radius, and h_{12} is a function that approximates the anisotropic interparticle clearance distance. η_{12} and χ_{12} characterize anisotropic interactions of particles due to their shapes and relative orientations, given by the following equations:

$$\eta_{12} = \sqrt{\frac{2s_1 s_2}{\det(\boldsymbol{G}_{12})}},\ s_i = (a_i b_i + c_i c_i)\sqrt{a_i b_i} \tag{6a}$$

where other terms are given by

$$h_{12} = r - \sigma_{12} \tag{6c}$$

$$\chi_{12} = \left(2\,\hat{\boldsymbol{r}}_{12}^{\top}\boldsymbol{B}_{12}^{-\top}\hat{\boldsymbol{r}}_{12}\right)^2 \tag{6b}$$

$$\sigma_{12} = \left(\frac{1}{2}\hat{\boldsymbol{r}}_{12}^{\top}\boldsymbol{G}_{12}^{-\top}\hat{\boldsymbol{r}}_{12}\right)^{-\frac{1}{2}},\ \hat{\boldsymbol{r}}_{12} = \frac{\boldsymbol{r}_{12}}{|\boldsymbol{r}_{12}|} \tag{6d}$$

$$\boldsymbol{G}_{12} = \boldsymbol{A}_1^{\top}\boldsymbol{S}_1^2\boldsymbol{A}_1 + \boldsymbol{A}_2^{\top}\boldsymbol{S}_2^2\boldsymbol{A}_2,\ \boldsymbol{S}_i = \mathrm{diag}(a_i,b_i,c_i) \tag{6e}$$

$$\boldsymbol{B}_{12} = \boldsymbol{A}_1^{\top}\boldsymbol{E}_1\boldsymbol{A}_1 + \boldsymbol{A}_2^{\top}\boldsymbol{E}_2\boldsymbol{A}_2,\ \boldsymbol{E}_i = \mathrm{diag}\left(\epsilon_{ia}^{-1/2},\epsilon_{ib}^{-1/2},\epsilon_{ic}^{-1/2}\right) \tag{6f}$$

Parameters a_i, b_i, and c_i describe the shape of particle i and ϵ_{ia}, ϵ_{ib}, and ϵ_{ic} are the depths of the potential wells in three principal orientations. $\boldsymbol{A}_1$ and $\boldsymbol{A}_2$ are the rotation matrices of the two interacting particles.

The GB potential is defined by 6 parameters that can be fitted to the PMFs from face−face and edge−edge configurations (a, c, ϵ_a, ϵ_c, and σ). Figure 6a,b compares the GB potential function with the nanoscale PMF curves assuming ellipsoidal particles with radius $2a = 2b = 1000$ Å. It is apparent that the GB potential provides only a first-order

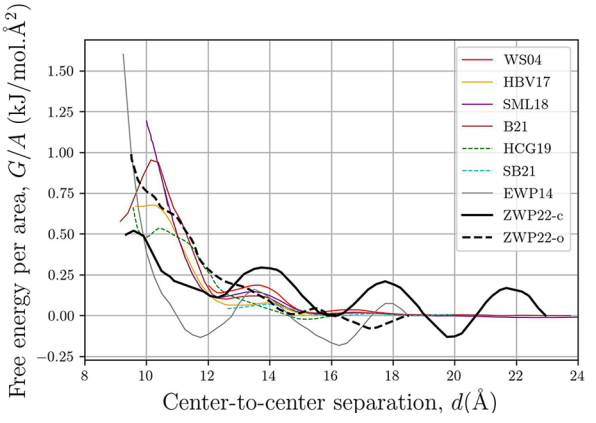

Figure 6. Compilation of PMFs for Na-smectite from various sources. All curves have been converted to free energy per area of the nanoplatelets. Open systems are indicated by dashed lines and closed systems by solid lines.

https://doi.org/10.1021/acs.langmuir.2c01632
Langmuir 2022, 38, 13065−13074

approximation to the nanoscale models. For illite PMFs, the parameters are chosen to fit the first dominant potential well, which is believed to govern the aggregation behavior.[9] The smectite F−F PMFs are observed to be repulsive in the general trend, and therefore a purely repulsive version of the Gay−Berne potential (referred to as GB-Repulsion in the following discussion) is used in fitting the results, i.e., eq 5a is replaced by

$$U' = 4\varepsilon \left[\left(\frac{\sigma}{h_{12} + \sigma}\right)^{12}\right] \eta_{12}\chi_{12} \tag{5b}$$

whereas all the rest of the model remain the same. GB repulsion has been used to study the aggregation behavior of mesoscale Kaolinite particles[57] with parameters based on DLVO theory.[58,59]

The parameters fitted with results from simulations with illite open and closed systems yield similar size of the particles (the fitted in-plane diameter is ∼6 Å more than the nominal diameter assumed value). This is due to the differences between the edges of the ellipsoidal particles and the cleaved atomistic structure. While the GB potential is able to represent the separation distance and depth of the attractive energy well, it notably overestimates repulsion at small separations (closed system, Figure 7a), tends to overestimate the width of the energy well (open system, Figure 7b), and does not describe the oscillating free energy field associated with different solvation states (both open and closed systems). In the case of smectite, GB repulsion captures very well the general trend of the F−F interaction as a first approximation but does not represent accurately the E−E interaction, which has a dominant potential well at ∼9 Å.

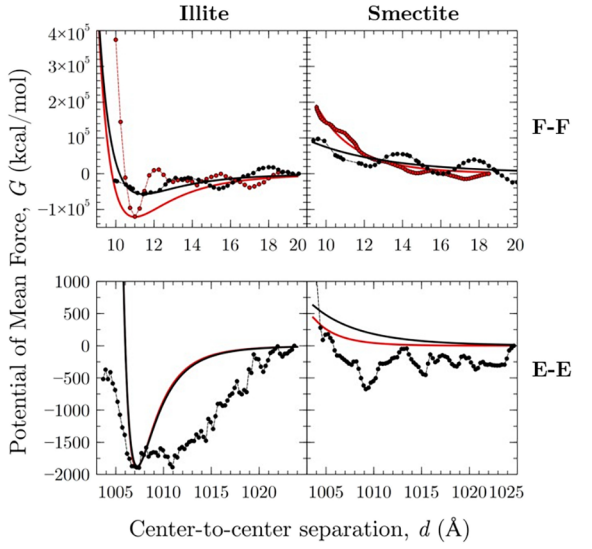

	Symbol	Type	a (Å)	c (Å)	εa	εc	σ (Å)
Closed fit		Illite	503.0	5.1	38	1160	10.2
		Smectite	428.8	7.5	11.9	205	55.0
Open fit		Illite	503.0	4.9	37	2357	9.8
		Smectite	546.0	6.2	11.9	261	26.2
Closed/E-E data							
Open data							

Figure 7. Fitting of Gay−Berne potential to PMF's for illite and Na-smectite platelets with a diameter of 1000 Å. In the fitting of smectite PMFs, two versions of GB potentials are used. The unit is defined by the parameter ϵ = 1 kcal/mol.

3.5.2. Improved Representation of PMFs. We have investigated the application of other potential functions to characterize meso-scale interactions between 2:1 clay particles. Masoumi and co-workers[60] observed oscillatory features in the intermolecular forces between calcium-silicate-hydrate (CSH) layers, similar to those found for illite. They attributed these effects to the presence of counterions and formation of layered interlayer water structure (referred to as solvation interaction). The model proposed that the potential energy can be divided into three parts, representing attraction, repulsion, and solvation interactions:

$$U = U_{attr} + U_{repl} + U_{solv} \tag{7a}$$

$$U_{attr} = -\frac{b_1}{(b_2 + r)^2} \tag{7b}$$

$$U_{repl} = b_3 \exp\left(-\frac{r}{b_4}\right) \tag{7c}$$

$$U_{solv} = -b_5 \sin\left[\frac{2\pi}{b_7}(r - b_6)\right] \exp\left(-\frac{r}{b_8}\right) \tag{7d}$$

where b_1 to b_8 are constants that are fitted to the PMF results obtained using the free energy perturbation method. In the original model, the solvation characteristic decay length in eq 7d was chosen to be the same as the wavelength of the sinusoidal part (i.e., $b_7 = b_8$). Here, we treat b_7 and b_8 as independent parameters for better matching to the computed PMFs.

Figure 8 shows that these potentials describe the PMF computed for the F−F open illite system with much higher fidelity than the GB potential and hence can provide a more complete representation for mesoscale modeling. Using this model, we are able to analyze the relative strength of different components of the PMF's for different configurations, as shown in Figure 9. The fitting is based on minimizing the cost function defined as:

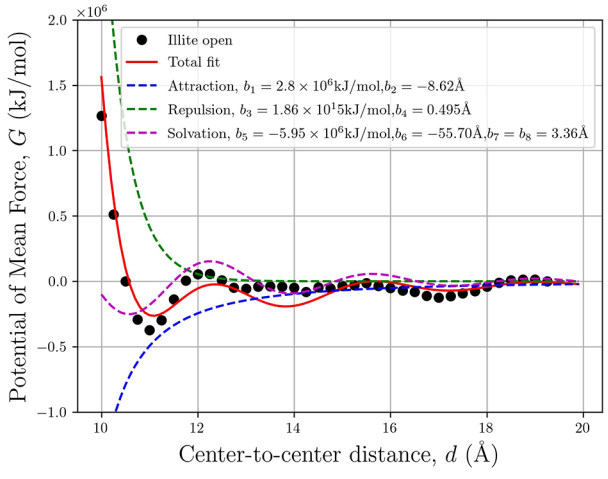

Figure 8. Illustration of potential function proposed by Masoumi and co-workers[60] for free energy in face−face simulations for illite.

https://doi.org/10.1021/acs.langmuir.2c01632
Langmuir 2022, 38, 13065−13074

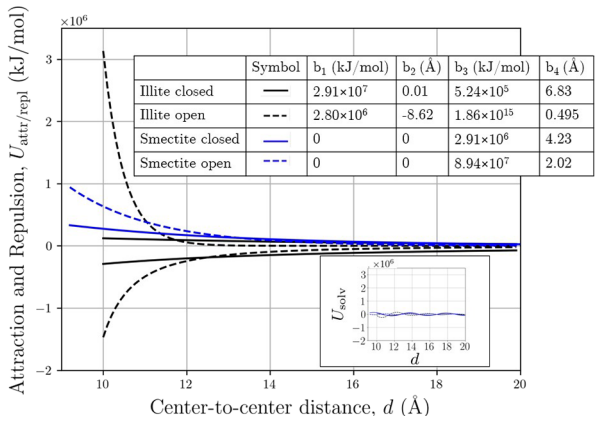

	Symbol	b_1 (kJ/mol)	b_2 (Å)	b_3 (kJ/mol)	b_4 (Å)
Illite closed	—	2.91×10^{7}	0.01	5.24×10^{5}	6.83
Illite open	- - -	2.80×10^{6}	-8.62	1.86×10^{15}	0.495
Smectite closed	—	0	0	2.91×10^{6}	4.23
Smectite open	- - -	0	0	8.94×10^{7}	2.02

(a) attractive and repulsive components of PMFs (eqns. 7b, 7c)

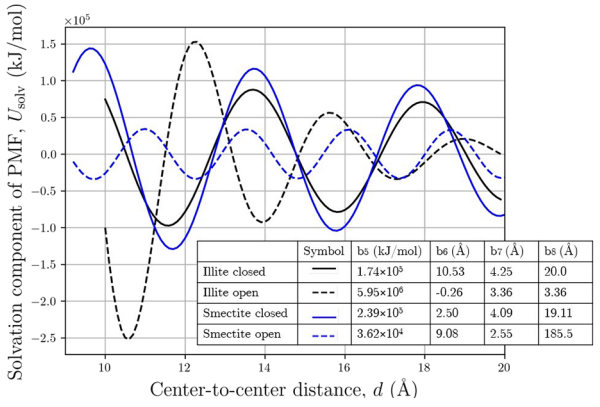

	Symbol	b_5 (kJ/mol)	b_6 (Å)	b_7 (Å)	b_8 (Å)
Illite closed	—	1.74×10^{5}	10.53	4.25	20.0
Illite open	- - -	5.95×10^{6}	-0.26	3.36	3.36
Smectite closed	—	2.39×10^{5}	2.50	4.09	19.11
Smectite open	- - -	3.62×10^{4}	9.08	2.55	185.5

(b) solvation component of the PMFs (eqn. 7c)

Figure 9. Components of F−F PMFs for illite closed/open (narrow) and smectite closed/open systems. The inset in panel (a) is the same content as in panel (b) but in the same scale as the attraction and repulsion plots for comparison.

$$F_{cost} = \sum_{i=1}^{n} [G(d_i) - \check{G}(d_i)]^2 \tag{8}$$

where $G(d_i)$ and $\check{G}(d_i)$ are the free energy for state with separation d_i from FEP calculation and estimated with Masoumi potential, respectively.

Based on the comparison between different components and configurations, we have the following observations:

1. Solvation interactions are much smaller than attraction and repulsion interactions. The former dominates interactions at large separation distance; the latter two dominate interactions at small separation.
2. Smectite PMFs have no overall attraction interactions.
3. Illite repulsion and solvation components have greater magnitude and shorter decay characteristic lengths (b_4 and b_8) than smectite.
4. Repulsion and attraction components have greater magnitude and shorter decay characteristic lengths for open than closed systems.

Solvation interaction is related to the formation of structured water layer that typically extends up to ~10 Å from the surface. Consequently, its influence on interaction at larger separation is stronger than repulsion and attraction interaction, which are mainly the collective behavior of short-range van der Waals and Coulombic interactions (Observation 1). In Section 3.3, we observed that high density layers of counterions near the surface of the primary illite particles and therefore illite tends to have stronger repulsion (and attraction) interactions that decays more rapidly with separation distance than smectite (Observations 2 and 3). Due to the presence of ion exclusion, open systems tend to have stronger near field interactions (repulsion and attraction) than closed systems where interlayer ions are confined during the simulations (Observation 4). The structure of counterions near the particle surface plays an important role in the PMF's between the particles.

3.5.3. Comparison between Masoumi and GB Potentials. Despite the power of Masoumi's model in accurately capturing the features of F−F interactions for Illite and Smectite particles, it is not readily integrated into a simple coarse-grained model for use in mesoscale simulations and face multiple technical difficulties. One way is to incorporate Masoumi's model in the GB potential as an improvement of the LJ distance-related term, i.e.,

$$U'' = u_{Masoumi}\eta_{12}\chi_{12} \tag{9}$$

However, F−F and E−E interactions differ in several aspects. In the case of illite, E−E interactions does not exhibit noticeable solvation interactions as in F−F interactions. For smectite, the F−F interactions are generally repulsive, but E−E interactions have a dominant potential well. This cannot be reconciled with a distance-related term $u_{Masoumi}$ that has parameters not related to the relative orientations of particles.

It is also possible to make a compromise between computational efficiency and accuracy through representing the coarse-grained particles as a collection of interaction sites and distinguish the sites into center and edge types, so that the differences between F−F and E−E interactions can be easily reconciled. Another benefit of this method is the ability to represent particle flexibility (in terms of tensile and flexural stiffness) through assigning bonds and bond angles among the interacting sites, to represent more features of the real clay platelets. Apart from the higher computational cost, another limitation is that it will introduce an artificial characteristic length related to the spacing between the interacting sites that may lead to unphysical results in mesoscale simulations.

GB potential has the benefit of computational efficiency and widespread prior usage.[9,57] As a first approximation, though not ideal in the case of smectite, it can very well capture the interactions between primary particles of illite (in terms of positions and depths of the potential wells). It also has the potential to be improved and modified to cope with various situations.

4. CONCLUSIONS

In response to the growing need to understand clay properties from a multiscale perspective, it is increasingly crucial to obtain reliable information about the interparticle interactions (Potential of Mean Force) and invent effective ways to carry the PMF to larger length scales (coarse-graining methods), which represent the basis for understanding macroscopic material behavior based on meso- and microscale properties. This work studied the PMF's between illite and smectite primary particles with confined and unconfined interlayer space (closed and open systems) through FEP calculations and compared the results with previous studies with other free energy calculation methods. Various coarse-graining methods

https://doi.org/10.1021/acs.langmuir.2c01632
Langmuir 2022, 38, 13065−13074

(GB potential and Masoumi potential) were also studied and evaluated. We find the following:

Smectite PMFs exhibit net repulsion for face−face interactions at $d \leq 16$ Å. This is consistent to the majority of the results from previous literature with various free energy calculation methods. In contrast, illite PMFs have dominant potential wells in the near field.

Oscillatory features were observed in the PMFs related to the layered structure of interplatelet water and were well described by the solvation potential proposed by Masoumi et al.[60]

Illite particles have more concentrated layers of counterions adsorbed to the surface than smectite. The differences qualitatively explain the differences in their PMF's and between open and closed systems.

Ion exclusions were observed in open systems of illite and smectite, which is the key feature distinguishing open systems from closed systems.

GB potential was found to be a good first order approximation capturing the physics of interparticle interactions.

■ ASSOCIATED CONTENT

Supporting Information

The Supporting Information is available free of charge at https://pubs.acs.org/doi/10.1021/acs.langmuir.2c01632.

CLAYFF force field; comparison; free energy perturbation method (PDF)

■ AUTHOR INFORMATION

Corresponding Author

Hejian Zhu − *Department of Civil and Environmental Engineering, Massachusetts Institute of Technology, Cambridge, Massachusetts 02139-4307, United States;* orcid.org/0000-0003-3652-1388; Email: patzhu@mit.edu

Authors

Andrew J. Whittle − *Department of Civil and Environmental Engineering, Massachusetts Institute of Technology, Cambridge, Massachusetts 02139-4307, United States*

Roland J.-M. Pellenq − *Laboratoire de Mécanique et Génie Civil, CNRS-Université de Montpellier, 34090 Montpellier, France; Epidapo, the joint CNRS/ George Washington University laboratory, IRL2006, Children's National Medical Center, Children's Research Institute, Washington, District of Columbia 20010, United States*

Complete contact information is available at: https://pubs.acs.org/10.1021/acs.langmuir.2c01632

Notes

The authors declare no competing financial interest.

■ ACKNOWLEDGMENTS

The authors acknowledge the support from National Science Foundation grant number: CMMI-**1702689**. The simulations in the works were conducted using resources at Extreme Science and Engineering Discovery Environment (XSEDE) Stampede2 at the Texas Advanced Computing Center (TACC) through allocation TG-MSS180023.

■ REFERENCES

(1) Garrels, R. M.; MacKenzie, F. T.*Evolution of Sedimentary Rocks*; W. W. Norton: New York, 1971.

(2) Sposito, G.*The Chemistry of Soils*; Oxford University Press: New York, 1989.

(3) Tester, C. C.; Aloni, S.; Gilbert, B.; Banfield, J. F. Short- and Long-Range Attractive Forces That Influence the Structure of Montmorillonite Osmotic Hydrates. *Langmuir* **2016**, *32*, 12039−12046.

(4) Nadeau, P. H. The Physical Dimension of Clay Fundamental Clay Particles. *Clay Miner.* **1985**, *20*, 499−514.

(5) Velde, B.; Meunier, A.*Development of Soils and Weathering Profile. In The Origin of Clay Minerals in Soils and Weathered Rock*; Springer: Berlin, Heidelberg, 2008.

(6) Cygan, R. T.; Liang, J. J.; Kalinichev, A. G. Molecular Models of Hydroxide, Oxyhydroxide, and Clay Phases and the Development of a General Force Field. *J. Phys. Chem. B* **2004**, *108*, 1255−1266.

(7) Berendsen, H. J. C.; Grigera, J. R.; Straatsma, T. P. The Missing Term in Effective Pair Potentials. *J. Phys. Chem.* **1987**, *91*, 6269−6271.

(8) Underwood, T. R.; Bourg, I. C. Large-Scale Molecular Dynamics Simulation of the Dehydration of a Suspension of Smectite Clay Nanoparticles. *J. Phys. Chem. C* **2020**, *124*, 3702−3714.

(9) Ebrahimi, D.; Whittle, A. J.; Pellenq, R. J.-M. Mesoscale Properties of Clay Aggregates from Potential of Mean Force Representation of Interactions between Nanoplatelets. *J. Chem. Phys.* **2014**, *140*, 154309.

(10) Ioannidou, K.; Krakowiak, K. J.; Bauchy, M.; Hoover, C. G.; Masoero, E.; Yip, S.; Ulm, F.-J.; Levitz, P.; Pellenq, R. J.-M.; Del Gado, E. Mesoscale Texture of Cement Hydrates. *Proc. Natl. Acad. Sci. U.S.A.* **2016**, *113*, 2029−2034.

(11) Orphen, H. V.; Fripiat, J.*Materials and Other Non-Metallic Minerals*; Pergamon Press, 1979.

(12) Newman, A. C. D.*Chemistry of Clays and Clay Minerals*; Longman Scientific & Technical, 1987.

(13) Mitchell, J. K.; Soga, K.*Fundamentals of Soil Behavior*; 3rd ed.; John Wiley & Sons, Ltd: Hoboken, 2005.

(14) Refson, K.; Park, S. H.; Sposito, G. Ab Initio Computational Crystallography of 2:1 Clay Minerals: 1.Pyrophyllite-1Tc. *J. Phys. Chem. B* **2003**, *107*, 13376−13383.

(15) Ferrage, E. Investigation of Smectite Hydration Properties by Modeling Experimental X-Ray Diffraction Patterns: Part I. Montmorillonite Hydration Properties. *Am. Mineral.* **2005**, *90*, 1358−1374.

(16) Ferrage, E.; Lanson, B.; Michot, L. J.; Robert, J. L. Hydration Properties and Interlayer Organization of Water and Ions in Synthetic Na-Smectite with Tetrahedral Layer Charge. *J. Phys. Chem. C* **2010**, *114*, 4515−4526.

(17) Ferrage, E.; Sakharov, B. A.; Michot, L. J.; Delville, A.; Bauer, A.; Lanson, B.; Grangeon, S.; Frapper, G.; Jiménez-Ruiz, M.; Cuello, G. J. Hydration Properties and Interlayer Organization of Water and Ions in Synthetic Na-Smectite with Tetrahedral Layer Charge. Part 2. Toward a Precise Coupling between Molecular Simulations and Diffraction Data. *J. Phys. Chem. C* **2011**, *115*, 1867−1881.

(18) Holmboe, M.; Wold, S.; Jonsson, M. Porosity Investigation of Compacted Bentonite Using XRD Profile Modeling. *J. Contam. Hydrol.* **2012**, *128*, 19−32.

(19) Saiyouri, N.; Tessier, D.; Hicher, P. Y. Experimental Study of Swelling in Unsaturated Compacted Clays. *Clay Miner.* **2004**, *39*, 469−479.

(20) Ebrahimi, D.; Pellenq, R. J. M.; Whittle, A. J. Nanoscale Elastic Properties of Montmorillonite upon Water Adsorption. *Langmuir* **2012**, *28*, 16855−16863.

(21) Shahsavari, R.; Pellenq, R. J.-M.; Ulm, F.-J. Empirical Force Fields for Complex Hydrated Calcio-Silicate Layered Materials. *Phys. Chem. Chem. Phys.* **2011**, *13*, 1002−1011.

(22) Newton, A. G.; Sposito, G. Molecular Dynamics Simulations of Pyrophyllite Edge Surfaces: Structure, Surface Energies, and Solvent Accessibility. *Clays Clay Miner.* **2015**, *63*, 277−289.

(23) Churakov, S. V. Ab Initio Study of Sorption on Pyrophyllite: Structure and Acidity of the Edge Sites. *J. Phys. Chem. B* **2006**, *110*, 4135−4146.
(24) Churakov, S. V. Structure and Dynamics of the Water Films Confined between Edges of Pyrophyllite: A First Principle Study. *Geochim. Cosmochim. Acta* **2007**, *71*, 1130−1144.
(25) Plimpton, S. Fast Parallel Algorithms for Short-Range Molecular Dynamics. *J. Comput. Phys.* **1995**, *117*, 1−19.
(26) Thompson, A. P.; Aktulga, H. M.; Berger, R.; Bolintineanu, D. S.; Brown, W. M.; Crozier, P. S.; In't Veld, P. J.; Kohlmeyer, A.; Moore, S. G.; Nguyen, T. D.; Shan, R.; Stevens, M. J.; Tranchida, J.; Trott, C.; Plimpton, S. J. LAMMPS - a Flexible Simulation Tool for Particle-Based Materials Modeling at the Atomic, Meso, and Continuum Scales. *Comput. Phys. Commun.* **2022**, *271*, No. 108171.
(27) Stukowski, A. Visualization and Analysis of Atomistic Simulation Data with OVITO-the Open Visualization Tool. *Modell. Simul. Mater. Sci. Eng.* **2010**, *18*, No. 015012.
(28) Hockney, R. W.; Eastwood, J. W.*Computer Simulation Using Particles*; 1988, DOI: 10.1887/0852743920.
(29) Shinoda, W.; Shiga, M.; Mikami, M. Rapid Estimation of Elastic Constants by Molecular Dynamics Simulation under Constant Stress. *Phys. Rev. B* **2004**, *69*, 16−18.
(30) Zwanzig, R. W. High-Temperature Equation of State by a Perturbation Method. I. Nonpolar Gases. *J. Chem. Phys.* **1954**, *22*, 1420−1426.
(31) Lee, C. Y.; Scott, H. L. The Surface Tension of Water: A Monte-Carlo Calculation Using an Umbrella Sampling Algorithm. *J. Chem. Phys.* **1980**, *73*, 4591.
(32) Chipot, A.; Pohorille, A.*Free Energy Calculation*; Springer, 2017.
(33) Ryckaert, J. P.; Ciccotti, G.; Berendsen, H. J. C. Numerical Integration of the Cartesian Equations of Motion of a System with Constraints: Molecular Dynamics of n-Alkanes. *J. Comput. Phys.* **1977**, *23*, 327−341.
(34) Bourg, I. C.; Lee, S. S.; Fenter, P.; Tournassat, C. Stern Layer Structure and Energetics at Mica-Water Interfaces. *J. Phys. Chem. C* **2017**, *121*, 9402−9412.
(35) Sakuma, H.; Kawamura, K. Structure and Dynamics of Water on Li+−, Na+−, K+-, Cs+−, H3O+-Exchanged Muscovite Surfaces: A Molecular Dynamics Study. *Geochim. Cosmochim. Acta* **2011**, *75*, 63−81.
(36) Boek, E. S.; Coveney, P. V.; Skipper, N. T. Monte Carlo Molecular Modeling Studies of Hydrated Li-, Na-, and K-Smectites: Understanding the Role of Potassium as a Clay Swelling Ihibitor. *J. Am. Chem. Soc.* **1995**, *117*, 12608−12617.
(37) Whitley, H. D.; Smith, D. E. Free Energy, Energy, and Entropy of Swelling in Cs-, Na-, and Sr-Montmorillonite Clays. *J. Chem. Phys.* **2004**, *120*, 5387−5395.
(38) Honorio, T.; Brochard, L.; Vandamme, M. Hydration Phase Diagram of Clay Particles from Molecular Simulations. *Langmuir* **2017**, *33*, 12766−12776.
(39) Brochard, L. Swelling of Montmorillonite from Molecular Simulations: Hydration Diagram and Confined Water Properties. *J. Phys. Chem. C* **2021**, *125*, 15527−15543.
(40) Svoboda, M.; Moučka, F.; Lísal, M. Saturated Aqueous NaCl Solution and Pure Water in Na-Montmorillonite Clay at Thermodynamic Conditions of Hydraulic Fracturing: Thermodynamics, Structure and Diffusion from Molecular Simulations. *J. Mol. Liq.* **2018**, *271*, 490−500.
(41) Leach, A.*Molecular Modelling: Principles and Applications*; Prentice Hall: Harlow, UK, 2001.
(42) Ho, T. A.; Criscenti, L. J.; Greathouse, J. A. Revealing Transition States during the Hydration of Clay Minerals. *J. Phys. Chem. Lett.* **2019**, *10*, 3704−3709.
(43) Shen, X.; Bourg, I. C. Molecular Dynamics Simulations of the Colloidal Interaction between Smectite Clay Nanoparticles in Liquid Water. *J. Colloid Interface Sci.* **2021**, *584*, 610−621.
(44) White, G. N.; Zelazny, L. Analysis and Implications of the Edge Structure of Dioctahedral Phyllosilicates. *Clays Clay Miner.* **1988**, *36*, 141.
(45) Drits, V. XRD Measurement of Mean Crystallite Thickness of Illite and Illite/Smectite: Reappraisal of the Kubler Index and the Scherrer Equation. *Clays Clay Miner.* **1997**, *45*, 461−475.
(46) Drits, V. A. XRD Measurement of Mean Thickness, Thickness Distribution and Strain for Illite and Illite-Smectite Crystallites by the Bertaut-Warren-Averbach Technique. *Clays Clay Miner.* **1998**, *46*, 38−50.
(47) Wang, H.; Zhou, J. Asymmetry of 1 Nm XRD Reflection and Measurement of Illite Crystallinity. *Acta Phys. Pol. A* **2016**, *130*, 886−888.
(48) Sugiura, M.; Sueyoshi, M.; Seike, R.; Hayashi, T.; Okada, T. Hydrated Silicate Layer Formation on Mica-Type Crystals. *Langmuir* **2020**, *36*, 4933−4941.
(49) Pavon, E.; Castro, M. A.; Naranjo, M.; Orta, M. M.; Pazos, M. C.; Alba, M. D. Hydration Properties of Synthetic High-Charge Micas Saturated with Different Cations: An Experimental Approach. *Am. Mineral.* **2013**, *98*, 394−400.
(50) Marcos, C.; Arango, Y.; Rodriguez, I. X-Ray Diffraction Studies of the Thermal Behaviour of Commercial Vermiculites. *Appl. Clay Sci.* **2009**, *42*, 368−378.
(51) Wang, Z.; Wang, H.; Cates, M. E. Elastic Properties of Solid Clays. *Geophysics* **2001**, *66*, 428−440.
(52) Ortega, J. A.; Ulm, F. J.; Abousleiman, Y. The Effect of the Nanogranular Nature of Shale on Their Poroelastic Behavior. *Acta Geotech.* **2007**, *2*, 155−182.
(53) Graham, S. P.; Rouainia, M.; Aplin, A. C.; Cubillas, P.; Fender, T. D.; Armitage, P. J. Geomechanical Characterisation of Organic-Rich Calcareous Shale Using AFM and Nanoindentation. *Rock Mech. Rock Eng.* **2021**, *54*, 303−320.
(54) Gay, J. G.; Berne, B. J. Modification of the Overlap Potential to Mimic a Linear Site-Site Potential. *J. Chem. Phys.* **1981**, *74*, 3316−3319.
(55) Berardi, R.; Fava, C.; Zannoni, C. A Gay-Berne Potential for Dissimilar Biaxial Particles. *Chem. Phys. Lett.* **1998**, *297*, 8−14.
(56) Everaers, R.; Ejtehadi, M. R. Interaction Potentials for Soft and Hard Ellipsoids. *Phys. Rev. E* **2003**, *67*, 8.
(57) Bandera, S.; Sullivan, C. O.; Tangney, P.; Angioletti-Uberti, S. Coarse-Grained Molecular Dynamics Simulations of Clay Compression. *Comput. Geotech.* **2021**, *138*, No. 104333.
(58) Derjaguin, B.; Landau, L. D. Theory of the Stability of Strongly Charged Lyophobic Sols and of the Adhesion of Strongly Charged Particles in Solution Sof Electrolytes. *Acta Phys. Chim. USSR* **1941**, *14*, 633.
(59) Verwey, E. J. W. Theory of the Stability of Lyophobic Colloids. *J. Phys. Colloid Chem.* **1947**, *51*, 631−636.
(60) Masoumi, S.; Valipour, H.; Abdolhosseini Qomi, M. J. Interparticle Interactions in Colloidal Systems: Toward a Comprehensive Mesoscale Model. *ACS Appl. Mater. Interfaces* **2017**, *9*, 27338−27349.
(61) Skipper, N. T.; Chang, F. C.; Sposito, G. Monte Carlo Simulation of Interlayer Molecular Structure in Swelling Clay Minerals. 1 Methodology. *Clays Clay Miner.* **1995**, *43*, 285−293.
(62) Gale, G. GULP: A Computer Program for the Symmetry-Adapted Simulation of Solids. *J. Chem. Soc., Faraday Trans.* **1997**, *93*, 629−637.